ARTICLE IN PRESS

Alexandria Engineering Journal (2016) xxx, xxx–xxx

HOSTED BY

ELSEVIER

Alexandria University

Alexandria Engineering Journal

www.elsevier.com/locate/aej
www.sciencedirect.com

ORIGINAL ARTICLE

A numerical study of unsteady non-Newtonian Powell-Eyring nanofluid flow over a shrinking sheet with heat generation and thermal radiation

T.M. Agbaje [a,b], S. Mondal [a,*], S.S. Motsa [a], P. Sibanda [a]

[a] School of Mathematics, Statistics and Computer Sciences, University of KwaZulu-Natal, Private Bag X01, Scottsville 3209, Pietermaritzburg, South Africa

[b] DST-NRF Centre of Excellence in Mathematical and Statistical Sciences (CoE-MaSS), Private Bag 3, Wits 2050, Johannesburg, South Africa

Received 5 May 2016; revised 7 September 2016; accepted 19 September 2016

KEYWORDS

Powell-Eyring nanofluid;
Shrinking sheet;
Non-similarity solution;
Multi-domain bivariate spectral quasilinearization method

Abstract In this paper we investigate the unsteady boundary-layer flow of an incompressible Powell-Eyring nanofluid over a shrinking surface. The effects of heat generation and thermal radiation on the fluid flow are taken into account. Numerical solutions of the nonlinear differential equations that describe the transport processes are obtained using a multi-domain bivariate spectral quasilinearization method. This innovative technique involves coupling bivariate Lagrange interpolation with quasilinearization. The solutions of the resulting system of equations are then obtained in a piecewise manner in a sequence of multiple intervals using the Chebyshev spectral collocation method. A parametric study shows how various parameters influence the flow and heat transfer processes. The validation of the results, and the method used here, has been achieved through a comparison of the current results with previously published results for selected parameter values. In general, an excellent agreement is observed. The results from this study show that the fluid parameters ε and δ reduce the flow velocity and the momentum boundary-layer thickness. The heat generation and thermal radiation parameters are found to enhance both the temperature and thermal boundary-layer thicknesses.

1. Introduction

The study of flow and transport processes in non-Newtonian fluids has gained much research attention in recent years due to the important use of various such fluids in industry, biological processes and chemical engineering. A few examples of such applications include in the manufacture of optical fibers and plastic polymers, clay coating and in cosmetic products. Due to the wide diversity of non-Newtonian fluids, the important rheological characteristics of such flows cannot be addressed by a single constitutive relation between the shear stress and the shear rate. Significant contributions to the study of non-Newtonian fluid models with a variety of rheological

* Corresponding author.
E-mail address: sabya.mondal.2007@gmail.com (S. Mondal).

Peer review under responsibility of Faculty of Engineering, Alexandria University.

http://dx.doi.org/10.1016/j.aej.2016.09.006
1110-0168 © 2016 Faculty of Engineering, Alexandria University. Production and hosting by Elsevier B.V.

properties have been made by Harris [1] and Bird et al. [2]. An interesting non-Newtonian fluid is the Powell-Eyring fluid, which, although very complex, has certain advantages over other non-Newtonian fluid models, Powell and Eyring [3] in some respects. These include the fact that the model is derived from kinetic theory of liquids instead of the empirical relation, and that the Powell-Eyring fluid model reduces to the Newtonian fluid for low and high shear rates. A common example of an Powell-Eyring fluid is human blood. Due to the importance of Powell-Eyring fluids, many researchers have studied different physical properties of Powell-Eyring fluids. These include the study of Malik et al. [4] who investigated mixed convection in an MHD Eyring-Powell nanofluid over a stretching sheet. They showed that the fluid was accelerated by increasing the Eyring-Powell parameter and the mixed convection parameter. Hayat et al. [5] investigated radiation effects on the flow of a Powell-Eyring fluid past an unsteady inclined stretching sheet with a non-uniform heat source/sink. They showed that the velocity and temperature profiles generally decrease with the unsteadiness parameter. An increase in the radiation parameter was shown to increase the heat flux from the plate, which in turn enhanced the fluid velocity and temperature.

The unsteady incompressible Eyring-Powell flow in a pipe with porous walls was investigated by Zaman et al. [6] using the homotopy analysis method. Series of solutions of an unsteady Eyring Powell nanofluid flow about a rotating cone were obtained by Nadeem and Saleem [7]. In their investigation, they observed that the nano particle volume fraction decreased with the particle Brownian motion and the Lewis number. Jalil et al. [8] found self-similar solutions for flow and heat transfer in an Powell-Eyring fluid flow over a moving surface with a variable surface temperature. Roşca and Pop [9] studied the boundary-layer flow and heat transfer in a Powell-Eyring fluid over a shrinking surface. In their study, numerical results were obtained using the Matlab inbuilt function bvp4c. They found dual solutions for negative values of the stretching parameter and stability analysis showed that the first (upper branch) solution was stable and physically realizable, while the second (lower branch) solution is not stable and, therefore, not physically possible. Other Powell-Eyring studies were carried out by Hayat et al. [10,11], Asmat et al. [12], Khan and Sultan [13], Nadeem and Saleem [14].

In the past few years, the study of the flow, and the thermophysical properties of nanofluids has become a topic of major interest due to the huge potential for the use of these fluids as efficient heat transfer fluids, and in some biomedical applications. The concept of a nanofluid was first proposed by Chol [15] when he showed that by adding a small quantity of nanoparticles to conventional heat transfer liquids, the thermal conductivity of the fluid improved by approximately a factor of two. A non-homogeneous two component equation for nanofluids was developed by Buongiorno [16]. He introduced seven slip mechanisms between nanoparticles and the base fluid. He took into account particle Brownian motion and thermophoresis and showed that Brownian motion and thermophoresis have significant influence on forced convection in nanofluids. Rohni et al. [17] used the shooting method to find a numerical solution of the equations for an unsteady shrinking surface with wall mass suction using the nanofluid model proposed by Buongiorno [16]. Zaimi et al. [18] used the Buongiorno model to investigate unsteady flow due to a contracting cylinder. The equations were solved using the shooting method. They obtained dual solutions for a certain range of the unsteadiness parameter and also observed that the skin friction coefficient, the Nusselt number and the Sherwood number decreased with increasing values of the unsteadiness parameter. Multiple solutions of MHD boundary layer flow and heat transfer behavior of nanofluids induced by a power-law stretching/shrinking permeable sheet with viscous dissipation were presented by Dhanai et al. [19] using the shooting method. They showed the existence of dual solutions for different flow parameters. Further, they found that viscous dissipation is important whereas the Brownian motion has negligible effect on the rate of heat transfer. Recently, Haroun et al. [20] used the spectral relaxation method to solve the equations that model the unsteady MHD mixed convection in a nanofluid due to a stretching or shrinking surface with suctionand/or injection. Their results showed that the skin friction factor increases with both an increase in the nanoparticle volume fraction and the stretching rate, and that an increase in the nanoparticle volume fraction leads to a reduction in the wall mass transfer rate. Numerical solutions of heat and mass transfer of nanofluid through an impulsively stretching vertical surface were presented by Haroun et al. [21]. Other recent studies of nanofluid flows include those by Haroun et al. [22], Dalir et al. [23], Abolbashari et al. [24], Heidary et al. [25], Mansur et al. [26], Haq et al. [27], Mehmood et al. [28], Sher Akbar et al. [29–32].

The study of unsteady Powell-Eyring Nanofluid has not been given much attention so far. The aim of this study was to investigate the flow of an unsteady Powell-Eyring nanofluid over a shrinking sheet with heat generation and thermal radiation effects. The traditional model of Jalil et al. [8] and Rosca and Pop [9] is revised to incorporate the effects of thermal radiation, heat generation, thermophoresis and Brownian motion. The equations are solved numerically using a multi-domain or multi-stage bivariate spectral quasilinearization method (MD-BSQLM). Examples of multi-interval methods that have been developed to solve IVPs include the piecewise spectral homotopy analysis [33,34], the piecewise homotopy perturbation method [35], the multi-stage differential transformation method [36,37], multistage Adomian decomposition method [38,39], the multi-stage quasilinearization method [40,41], and multistage spectral relaxation method [42,43]. The MD-BSQLM is a novel technique that has not been used to solve systems of nonlinear partial differential equations. In this investigation, we extend the use of the method to systems of nonlinear partial differential equations. The multi-domain bivariate spectral quasilinearization method is based on linearizing the governing nonlinear system of PDEs using the Newton–Raphson based quasilinearization method of Bellman and Kalaba [47] and then integrating the resulting equation in multiple sub-intervals using the Chebyshev spectral collocation method with Lagrange interpolation polynomials as basis functions. The Chebyshev spectral collocation method with the Lagrange interpolation polynomials is applied on the linearized nonlinear systems of partial differential equations independently in both space and time direction. These useful features of the MD-BSQLM enable the approach to yield a very accurate solution and lead to significant computational time saving. The approach has a much better region of convergence for the approximate solution when compared to other Chebyshev spectral collocation based methods such as bivariate spectral homotopy analysis method [44], bivariate

Please cite this article in press as: T.M. Agbaje et al., A numerical study of unsteady non-Newtonian Powell-Eyring nanofluid flow over a shrinking sheet with heat generation and thermal radiation, Alexandria Eng. J. (2016), http://dx.doi.org/10.1016/j.aej.2016.09.006

Chebyshev spectral collocation quasilinearization method [45], bivariate spectral relaxation method [46], among others. These Chebyshev spectral collocation based methods remain to be tested on a wider range of problems that model real phenomena in engineering and science. The new approach yields accurate solutions with significant computational time savings. In order to demonstrate the accuracy of the method, a comparison with previously published results of Jalil et al. [8], Rosca and Pop [9] and Bachok et al. [48] has been made and our results are found to be in an excellent agreement.

2. Mathematical formulation

We consider an unsteady, two-dimensional flow of an incompressible Powell-Eyring nanofluid over a permeable surface coinciding with the axis $y = 0$. The flow is confined to $y > 0$, where y is measured in the normal direction to the shrinking surface. The constant mass flux velocity is v_0 with $v_0 < 0$ for suction, and $v_0 > 0$ for injection or withdrawal of the fluid. The surface temperature at the plate is $T_w(x)$ and in the ambient fluid this is T_∞. The ambient concentration is C_∞. The flow geometry is shown in Fig. 1.

Under these conditions, the dimensionless Powell-Eyring nanofluid boundary layer equations are as follows (see Jalil et al. [8], Rosca and Pop [9]):

$$\frac{\partial u}{\partial x} + \frac{\partial v}{\partial y} = 0, \tag{1}$$

$$\frac{\partial u}{\partial t} + u\frac{\partial u}{\partial x} + v\frac{\partial u}{\partial y} = u_e\frac{du_e}{dx} + (1+\varepsilon)\frac{\partial^2 u}{\partial y^2} - \varepsilon\delta\left(\frac{\partial u}{\partial y}\right)^2\left(\frac{\partial^2 u}{\partial y^2}\right), \tag{2}$$

$$\frac{\partial T}{\partial t} + u\frac{\partial T}{\partial x} + v\frac{\partial T}{\partial y} = \frac{\alpha_m}{\rho c_f}\frac{\partial^2 T}{\partial y^2} + \frac{Q_0}{\rho c_f}(T - T_\infty) - \frac{1}{\rho c_f}\frac{\partial q_r}{\partial y} + \tau\left[D_B\frac{\partial C}{\partial y}\frac{\partial T}{\partial y} + \frac{D_T}{T_\infty}\left(\frac{\partial T}{\partial y}\right)^2\right], \tag{3}$$

$$\frac{\partial C}{\partial t} + u\frac{\partial C}{\partial x} + v\frac{\partial C}{\partial y} = \frac{D_B}{v}\frac{\partial^2 C}{\partial y^2} + \frac{D_T}{T_\infty}\frac{\partial^2 T}{\partial y^2}, \tag{4}$$

subject to the initial and boundary conditions:

$$\begin{aligned} &t < 0: \quad v = u = 0, \quad T = T_w(x,t), \quad C = C_w(x,t), \quad \text{for any } x, y \\ &t \geqslant 0: \quad v = s v_w(x,t), \quad u = \lambda u_w(x,t), \quad T = T_w(x,t), \\ &D_B\frac{\partial C}{\partial y} + \frac{D_T}{T_\infty}\frac{\partial T}{\partial y} = 0, \quad \text{at} \quad y = 0, \\ &u = u_e(x,t), \quad T \to T_\infty, \quad C \to C_\infty, \quad \text{as} \quad y \to \infty, \end{aligned} \tag{5}$$

where t is the time, u and v are the velocity components along x- and y-axis, T and C are the fluid temperature and concentration respectively, ε and δ are Powell-Eyring fluid parameters, α_m is the thermal diffusivity, ρ is the density of the fluid, c_f is the specific heat at constant pressure, Q_0 is the heat generation constant, q_r is the radiation heat flux, $\tau = \frac{(\rho c)_{np}}{(\rho c)_f}$ is the ratio of the heat capacity of the nanoparticle material and the heat capacity of the fluid (see Oyelakin et al. [49]), D_B is the Brownian diffusion coefficient, D_T is the thermophoresis diffusion coefficient, λ is the dimensionless stretching/shrinking parameter with $\lambda > 0$ for a stretching surface and $\lambda < 0$ for a shrinking surface, and s is the dimensionless mass flux parameter with $s > 0$ for suction and $s < 0$ for injection respectively. These are defined as follows:

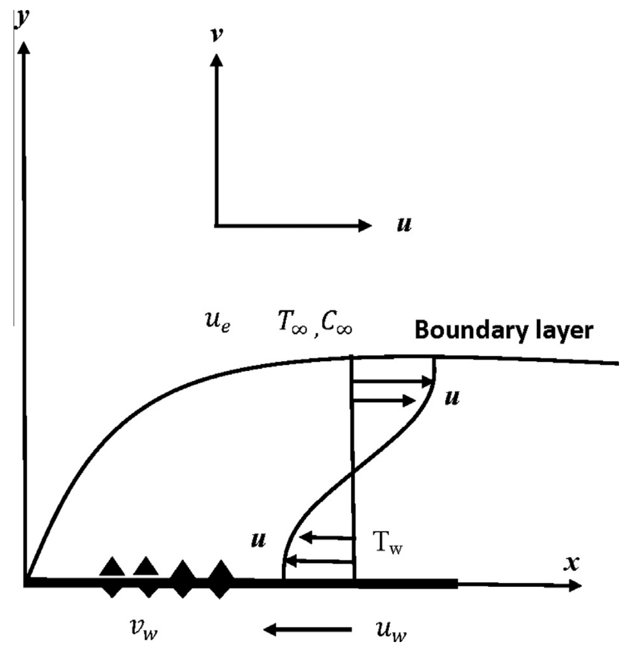

Fig. 1 Physical model of the flow.

$$\varepsilon = \frac{1}{\rho v\beta C_1}, \quad \delta = \frac{a^3}{2vLC_1^2}, \quad \lambda = \frac{c}{a}, \quad s = \frac{v_0}{a}\left(\frac{aL}{v}\right)^{1/2},$$

where ε and δ are Powell-Eyring fluid parameters, C_1 and β are the material parameters, ρ is the density, v is the kinematic viscosity and L is the length characteristics of the stretching/shrinking surface. Following Rosca and Pop [9], it is assumed that $u_w(x,t)$, $u_e(x,t)$ and $v_w(x,t)$ have the following forms:

$$u_w(x,t) = x^{1/3}, \quad u_e(x,t) = x^{1/3}, \quad v_w(x,t) = x^{-1/3}. \tag{6}$$

The following similarity variables are then introduced:

$$\psi = x^{2/3}f(\eta,\xi), \quad \xi = x^{-2/3}t, \quad \eta = x^{-1/3}y,$$
$$\theta(\xi,\eta) = \frac{T - T_\infty}{T_w - T_\infty}, \quad \phi(\xi,\eta) = \frac{C - C_\infty}{C_w - C_\infty}, \tag{7}$$

where ψ is the stream function such that

$$u = \frac{\partial\psi}{\partial y} \quad \text{and} \quad v = -\frac{\partial\psi}{\partial x}.$$

Substituting Eq. (6) into Eqs. (2)–(4), gives the following set of partial differential equations:

$$(1+\varepsilon)f''' + \frac{2}{3}ff'' + \frac{1}{3}(1 - f'^2) - \varepsilon\delta f'''(f'')^2 = \frac{\partial f'}{\partial\xi} - \frac{2}{3}\xi\left[f'\frac{\partial f'}{\partial\xi} - f''\frac{\partial f}{\partial\xi}\right], \tag{8}$$

$$\frac{1}{Pr}(1+N_R)\theta'' + \frac{2}{3}f\theta' + He\theta + N_b\theta'\phi' + N_t\theta'^2 = \frac{\partial\theta}{\partial\xi} - \frac{2}{3}\xi\left[f'\frac{\partial\theta}{\partial\xi} - \theta'\frac{\partial f}{\partial\xi}\right], \tag{9}$$

$$\phi'' + \frac{2}{3}Scf\phi' + \frac{N_t}{N_b}\theta'' = Sc\frac{\partial\phi}{\partial\xi} - \frac{2}{3}Sc\xi\left[f'\frac{\partial\phi}{\partial\xi} - \phi'\frac{\partial f}{\partial\xi}\right]. \tag{10}$$

The boundary condition (5) becomes:

$$f(0,\xi)=f_w,\quad f'(0,\xi)=\lambda,\quad f'(\infty,\xi)=1,$$
$$\theta(0,\xi)=1,\quad \theta(\infty,\xi)=0, \tag{11}$$
$$N_b\phi'(0,\xi)+N_t\theta'(0,\xi)=0,\quad \phi(\infty,\xi)=0.$$

In the above equations, prime denotes differentiation with respect to η, $f_w=-3s/2$ is the constant suction parameter ($f_w>0$) or injection ($f_w<0$). Other non-dimensional parameters appearing in Eqs. (8)–(11) are Pr which is the Prandtl number, N_R is the thermal radiation parameter, N_b is the Brownian motion parameter, N_t is the thermophoresis parameter, and He is the heat generation parameter. These parameters are mathematically defined as follows:

$$Pr=\frac{\rho c_f}{\alpha_m},\quad N_R=\frac{16\sigma^* T_\infty^3}{3\rho c_f k^*\alpha_m},\quad N_b=\tau D_B(C_w-C_\infty),$$
$$N_t=\tau\frac{D_T}{T_\infty}(T_w-T_\infty),\quad He=\frac{Q_0}{\rho c_f x^{-2/3}},\quad Sc=\frac{v}{D_B}, \tag{12}$$

3. Method of solution

In this section, we give a brief description of how the multi-domain (or piecewise or multi-stage) bivariate spectral quasi-linearization method (MD-BSQLM) is being used to solve Eqs. (8)–(10). The method is applied only in the ξ direction. In the MD-BSQLM, we first linearize Eqs. (8)–(10) using the quasilinearization (QLM) of Bellman and Kalaba [47]. Applying the QLM on (8)–(10) gives the following:

$$a_{0,r}(\eta,\xi)f'''_{r+1}+a_{1,r}(\eta,\xi)f''_{r+1}+a_{2,r}(\eta,\xi)f'_{r+1}+a_{3,r}(\eta,\xi)f_{r+1}$$
$$+a_{4,r}(\eta,\xi)\frac{\partial f'_{r+1}}{\partial\xi}+a_{5,r}(\eta,\xi)\frac{\partial f_{r+1}}{\partial\xi}=R_{1,r}(\eta,\xi), \tag{13}$$

$$b_{0,r}(\eta,\xi)\theta''_{r+1}+b_{1,r}(\eta,\xi)\theta'_{r+1}+b_{2,r}(\eta,\xi)\theta_{r+1}$$
$$+b_{3,r}(\eta,\xi)\frac{\partial\theta_{r+1}}{\partial\xi}+b_{4,r}(\eta,\xi)f'_{r+1}+b_{5,r}(\eta,\xi)f_{r+1}$$
$$+b_{6,r}(\eta,\xi)\frac{\partial f_{r+1}}{\partial\xi}+b_{7,r}(\eta,\xi)\phi'_{r+1}=R_{2,r}(\eta,\xi), \tag{14}$$

$$c_{0,r}(\eta,\xi)\phi''_{r+1}+c_{1,r}(\eta,\xi)\phi'_{r+1}+c_{2,r}(\eta,\xi)\phi_{r+1}$$
$$+c_{3,r}(\eta,\xi)\frac{\partial\phi_{r+1}}{\partial\xi}+c_{4,r}(\eta,\xi)f'_{r+1}+c_{5,r}(\eta,\xi)f_{r+1}$$
$$+c_{6,r}(\eta,\xi)\frac{\partial f_{r+1}}{\partial\xi}+c_{7,r}(\eta,\xi)\theta''_{r+1}=R_{3,r}(\eta,\xi), \tag{15}$$

$$f_{r+1}(0,\xi)=f_w,\quad f'_{r+1}(0,\xi)=\lambda,\quad f'_{r+1}(\infty,\xi)=1,$$
$$\theta_{r+1}(0,\xi)=1,\quad \theta_{r+1}(\infty,\xi)=0,$$
$$N_b\phi'_{r+1}(0,\xi)+N_t\theta'_{r+1}(0,\xi)=0,\quad \phi_{r+1}(\infty,\xi)=0, \tag{16}$$

where

$$a_{0,r}=(1+\varepsilon)-\varepsilon\delta(fr'')^2,\quad a_{1,r}=-2\varepsilon\delta fr''fr'''-\frac{2}{3}\xi\frac{\partial f_r}{\partial\xi}+\frac{2}{3}f_r,$$
$$a_{3,r}=\frac{2}{3}f''_r,$$
$$a_{4,r}=-1+\frac{2}{3}\xi f'_r,\quad a_{5,r}=-\frac{2}{3}\xi f''_r,$$
$$b_{0,r}=(1+N_R),\quad b_{1,r}=\frac{2}{3}Prf_r+N_bPr\phi'_r+2N_tPr\theta'_r$$
$$-\frac{2}{3}Pr\xi\frac{\partial f_r}{\partial\xi},\quad b_{2,r}=HePr,$$
$$b_{3,r}=\frac{2}{3}Pr\xi f'_r-Pr,\quad b_{4,r}=\frac{2}{3}Pr\xi\frac{\partial\theta}{\partial\xi},\quad b_{5,r}=\frac{2}{3}Pr\theta'_r,$$
$$b_{6,r}=-\frac{2}{3}Pr\xi\theta'_r,\quad b_{7,r}=N_bPr\theta'_r,$$
$$c_{0,r}=1,\quad c_{1,r}=\frac{2}{3}Scf_r-\frac{2}{3}Sc\xi\frac{\partial f_r}{\partial\xi},\quad c_{2,r}=0,$$
$$c_{3,r}=\frac{2}{3}Sc\xi f'_r-Sc,\quad c_{4,r}=\frac{2}{3}Sc\xi\frac{\partial\phi}{\partial\xi},$$
$$c_{5,r}=\frac{2}{3}Sc\phi'_r,\quad c_{6,r}=-\frac{2}{3}Sc\xi\phi'_r,\quad c_{7,r}=\frac{N_b}{N_t},$$
$$R_{1,r}=\frac{2}{3}f_rf''_r-\frac{1}{3}-2\varepsilon\delta\left(f''_r\right)^2f'''_r+\frac{2}{3}\xi f'_r\frac{\partial f'_r}{\partial\xi}-\frac{2}{3}\xi f''_r\frac{\partial f_r}{\partial\xi}-\frac{1}{3}\left(f'_r\right)^2$$
$$R_{2,r}=\frac{2}{3}Prf_r\theta'_r+N_bPr\theta'_r\phi'_r+N_tPr\left(\theta'_r\right)^2+\frac{2}{3}Pr\xi f'_r\frac{\partial\theta_r}{\partial\xi}$$
$$-\frac{2}{3}Pr\xi\theta'_r\frac{\partial f_r}{\partial\xi}$$
$$R_{3,r}=\frac{2}{3}Scf_r\phi'_r+\frac{2}{3}Sc\xi f'_r\frac{\partial\phi_r}{\partial\xi}-\frac{2}{3}Sc\xi\phi'_r\frac{\partial f_r}{\partial\xi}. \tag{17}$$

No, let $\xi\in\Omega$, where $\Omega\in[0,T]$ and the domain Ω is decomposed into p non-overlapping intervals as follows:

$$\Omega_m=[\xi_{m-1},\xi_m],\quad \xi_{m-1}<\xi_m,\quad \xi_0=0,\quad \xi_p=T,$$
$$m=1,2,\cdots,p. \tag{18}$$

The PDEs are solved independently at each of the p sub-intervals. Once the solution at the first sub-interval has been computed, the new solutions at the subsequent mth interval are computed using the solution at the right hand boundary of the $m-1$th interval as an initial solution. In the mth sub-interval, we solve the following:

$$a^{(m)}_{0,r}f'''^{(m)}_{r+1}+a^{(m)}_{1,r}f''^{(m)}_{r+1}+a^{(m)}_{2,r}f'^{(m)}_{r+1}+a^{(m)}_{3,r}f^{(m)}_{r+1}+a^{(m)}_{4,r}\frac{\partial f'^{(m)}_{r+1}}{\partial\xi}$$
$$+a^{(m)}_{5,r}\frac{\partial f^{(m)}_{r+1}}{\partial\xi}=R^{(m)}_{1,r}, \tag{19}$$

$$b^{(m)}_{0,r}\theta''^{(m)}_{r+1}+b^{(m)}_{1,r}\theta'^{(m)}_{r+1}+b^{(m)}_{2,r}\theta^{(m)}_{r+1}+b^{(m)}_{3,r}\frac{\partial\theta^{(m)}_{r+1}}{\partial\xi}+b^{(m)}_{4,r}f'^{(m)}_{r+1}$$
$$+b^{(m)}_{5,r}f^{(m)}_{r+1}+b^{(m)}_{6,r}\frac{\partial f^{(m)}_{r+1}}{\partial\xi}+b^{(m)}_{7,r}\phi'^{(m)}_{r+1}=R^{(m)}_{2,r}, \tag{20}$$

$$c^{(m)}_{0,r}\phi''^{(m)}_{r+1}+c^{(m)}_{1,r}\phi'^{(m)}_{r+1}+c^{(m)}_{2,r}\phi^{(m)}_{r+1}+c^{(m)}_{3,r}\frac{\partial\phi^{(m)}_{r+1}}{\partial\xi}+c^{(m)}_{4,r}f'^{(m)}_{r+1}$$
$$+c^{(m)}_{5,r}f^{(m)}_{r+1}+c^{(m)}_{6,r}\frac{\partial f^{(m)}_{r+1}}{\partial\xi}+c^{(m)}_{7,r}\theta''^{(m)}_{r+1}=R^{(m)}_{3,r}, \tag{21}$$

subject to the boundary conditions

$$f^{(m)}_{r+1}(0,\xi)=f_w,\quad f'^{(m)}_{r+1}(0,\xi)=\lambda,\quad f'^{(m)}_{r+1}(\infty,\xi)=1,$$
$$\theta^{(m)}_{r+1}(0,\xi)=1,\quad \theta^{(m)}_{r+1}(\infty,\xi)=0, \tag{22}$$
$$N_b\phi'^{(m)}_{r+1}(0,\xi)+N_t\theta'^{(m)}_{r+1}(0,\xi)=0,\quad \phi^{(m)}_{r+1}(\infty,\xi)=0.$$

A suitable initial condition to begin the piecewise iteration scheme in the first sub-interval is the one that satisfies the boundary conditions (15). Initial condition at the subsequent sub-intervals is given by the continuity conditions:

$$f^{(m)}(\eta,\xi_{m-1})=f^{(m-1)}(\eta,\xi_{m-1}),$$
$$\theta^{(m)}(\eta,\xi_{m-1})=\theta^{(m-1)}(\eta,\xi_{m-1}), \tag{23}$$
$$\phi^{(m)}(\eta,\xi_{m-1})=\phi^{(m-1)}(\eta,\xi_{m-1}).$$

Please cite this article in press as: T.M. Agbaje et al., A numerical study of unsteady non-Newtonian Powell-Eyring nanofluid flow over a shrinking sheet with heat generation and thermal radiation, Alexandria Eng. J. (2016), http://dx.doi.org/10.1016/j.aej.2016.09.006

The physical domains in η and ξ are first transformed to the computational domain $(x, t) \in [-1, 1] \times [-1, 1]$ at each sub-interval using the linear transformation:

$$\eta = \frac{Lx}{2}(1 + x), \quad \xi = \frac{1}{2}(\xi_m - \xi_{m-1})t + \frac{1}{2}(\xi_m + \xi_{m-1}), \tag{24}$$

where Lx is a number large enough to approximate conditions at infinity in η. The collocation points are the Chebyshev-Gauss-Lobatto nodes defined in [50,51] by

$$x_i = \cos\left(\frac{\pi i}{N_x}\right), t_j = \cos\left(\frac{\pi j}{N_t}\right), \; i = 0, 1, \ldots, N_x,$$
$$j = 0, 1, \ldots, N_t, \; x \in [-1, 1], \; t \in [-1, 1], \tag{25}$$

where $(N_x + 1)$ and $(N_t + 1)$ are the total number of collocation points in η- and ξ-directions respectively. Suppose that the solutions f, θ and ϕ can be approximated at each sub-interval by a bivariate Lagrange interpolation polynomial of the form:

$$\begin{aligned}
f^{(m)}(\eta, \xi) &\approx F^{(m)}(x, t) = \sum_{p=0}^{N_x}\sum_{q=0}^{N_t} F^{(m)}(x_p, t_q)L_p(x)L_q(t) \\
\theta^{(m)}(\eta, \xi) &\approx \Theta^{(m)}(x, t) = \sum_{p=0}^{N_x}\sum_{q=0}^{N_t} \Theta^{(m)}(x_p, t_q)L_p(x)L_q(t) \\
\phi^{(m)}(\eta, \xi) &\approx \Phi^{(m)}(x, t) = \sum_{p=0}^{N_x}\sum_{q=0}^{N_t} \Phi^{(m)}(x_p, t_q)L_p(x)L_q(t),
\end{aligned} \tag{26}$$

where the functions $L_p(x)$ and $L_q(t)$ are the Lagrange cardinal polynomials defined as

$$L_p(x) = \prod_{\substack{i=0\\ i\neq k}}^{N_x} \frac{x - x_k}{x_i - x_k}, \quad L_q(t) = \prod_{\substack{j=0\\ j\neq k}}^{N_t} \frac{t - t_k}{t_j - t_k}, \tag{27}$$

with

$$L_p(x_k) = \delta_{ik} = \begin{cases} 0 & \text{if } i \neq k \\ 1 & \text{if } i = k \end{cases}, \quad L_q(t_k) = \delta_{jk} = \begin{cases} 0 & \text{if } j \neq k \\ 1 & \text{if } j = k \end{cases}$$

The first spatial derivatives of f, θ, and ϕ with respect to η at the Chebyshev-Gauss-Lobatto points (x_i, t_j) for $i = 0, 1, 2, \ldots, N_x$ are evaluated as follows:

$$\begin{aligned}
\frac{\partial f^{(m)}}{\partial \eta}(x_i, t_j) &= \sum_{p=0}^{N_x}\sum_{q=0}^{N_t} F^{(m)}(x_p, t_q)\frac{dL_p(x_i)}{dx}L_p(t_j) = \sum_{p=0}^{N_x} F^{(m)}(x_p, t_j) \\
&\times \frac{dL_p(x_i)}{dx} = \sum_{p=0}^{N_x}\left(\frac{2}{L_x}\right)\widehat{D}_{i,p}F^{(m)}(x_p, t_j) = \left(\frac{2}{L_x}\right)\hat{\mathbf{D}}\mathbf{F}_j^{(m)} = \mathbf{D}\mathbf{F}_j^{(m)}, \\
\frac{\partial \theta^{(m)}}{\partial \eta}(x_i, t_j) &= \sum_{p=0}^{N_x}\sum_{q=0}^{N_t} \Theta^{(m)}(x_p, t_q)\frac{dL_p(x_i)}{dx}L_p(t_j) \\
&= \sum_{p=0}^{N_x} \Theta^{(m)}(x_p, t_j)\frac{dL_p(x_i)}{dx} = \sum_{p=0}^{N_x}\left(\frac{2}{L_x}\right)\widehat{D}_{i,p}\Theta^{(m)}(x_p, t_j) \\
&= \left(\frac{2}{L_x}\right)\hat{\mathbf{D}}\mathbf{\Theta}_j^{(m)} = \mathbf{D}\mathbf{\Theta}_j^{(m)}, \\
\frac{\partial \phi^{(m)}}{\partial \eta}(x_i, t_j) &= \sum_{p=0}^{N_x}\sum_{q=0}^{N_t} \Phi^{(m)}(x_p, t_q)\frac{dL_p(x_i)}{dx}L_p(t_j) \\
&= \sum_{p=0}^{N_x} \Phi^{(m)}(x_p, t_j)\frac{dL_p(x_i)}{dx} = \sum_{p=0}^{N_x}\left(\frac{2}{L_x}\right)\widehat{D}_{i,p}\Phi^{(m)}(x_p, t_j) \\
&= \left(\frac{2}{L_x}\right)\hat{\mathbf{D}}\mathbf{\Phi}_j^{(m)} = \mathbf{D}\mathbf{\Phi}_j^{(m)},
\end{aligned} \tag{28}$$

where $\hat{\mathbf{D}} = L_x\mathbf{D}/2$ is the standard first derivative Chebyshev differentiation matrix of size $(N_x + 1) \times (N_x + 1)$ as defined in Trefethen [50]. The vectors $\mathbf{F}_j^{(m)}$, $\mathbf{\Theta}_j^{(m)}$, $\mathbf{\Phi}_j^{(m)}$ are defined as

$$\begin{aligned}
\mathbf{F}_j^{(m)} &= \left[F(\eta_0, \xi_j), F(\eta_1, \xi_j) \cdot F(\eta_{N_x}, \xi_j)\right]^T, \\
\mathbf{\Theta}_j^{(m)} &= \left[\Theta(\eta_0, \xi_j), \Theta(\eta_1, \xi_j) \cdot \Theta(\eta_{N_x}, \xi_j)\right]^T, \\
\mathbf{\Phi}_j^{(m)} &= \left[\Phi(\eta_0, \xi_j), \Phi(\eta_1, \xi_j) \cdot \Phi(\eta_{N_x}, \xi_j)\right]^T,
\end{aligned}$$

and the superscript T here denotes matrix transpose. The nth order derivative of f, θ and ϕ with respect to η are approximated using the matrix product as

$$\begin{aligned}
\frac{\partial^n F^{(m)}}{\partial \eta^n}(x_i, t_j) &= \mathbf{D}^{(n)}\mathbf{F}_j^{(m)} \\
\frac{\partial^n \Theta^{(m)}}{\partial \eta^n}(x_i, t_j) &= \mathbf{D}^{(n)}\mathbf{\Theta}_j^{(m)}, \\
\frac{\partial^n \Phi^{(m)}}{\partial \eta^n}(x_i, t_j) &= \mathbf{D}^{(n)}\mathbf{\Phi}_j^{(m)}.
\end{aligned} \tag{29}$$

The spatial derivatives of f, θ and ϕ are evaluated at the Chebyshev-Gauss-Lobatto points (x_i, t_j) for $j = 0, 1, 2, \ldots, N_t$ as

$$\begin{aligned}
\frac{\partial F^{(m)}}{\partial \xi}(x_i, t_j) &= \sum_{p=0}^{N_x}\sum_{q=0}^{N_t} F^{(m)}(x_p, t_q)L_p(x_i)\frac{dL_q(t_j)}{dt} \\
&= \sum_{q=0}^{N_t} F^{(m)}(x_i, t_q)\frac{dL_q(t_j)}{dt} \sum_{q=0}^{N_t}\left(\frac{2}{\xi_m - \xi_{m-1}}\right)\hat{d}_{j,q}F^{(m)}(x_i, t_q) \\
&= \sum_{q=0}^{N_t}\left(\frac{2}{\xi_m - \xi_{m-1}}\right)\hat{d}_{j,q}F_q^{(m)} = \sum_{q=0}^{N_t} d_{j,q}F_q^{(m)}, \\
\frac{\partial \Theta^{(m)}}{\partial \xi}(x_i, t_j) &= \sum_{p=0}^{N_x}\sum_{q=0}^{N_t} \Theta^{(m)}(x_p, t_q)L_p(x_i)\frac{dL_q(t_j)}{dt} \\
&= \sum_{q=0}^{N_t} \Theta^{(m)}(x_i, t_q)\frac{dL_q(t_j)}{dt} \sum_{q=0}^{N_t}\left(\frac{2}{\xi_m - \xi_{m-1}}\right)\hat{d}_{j,q}\Theta^{(m)}(x_i, t_q) \\
&= \sum_{q=0}^{N_t}\left(\frac{2}{\xi_m - \xi_{m-1}}\right)\hat{d}_{j,q}\Theta_q^{(m)} = \sum_{q=0}^{N_t} d_{j,q}\Theta_q^{(m)}, \\
\frac{\partial \Phi^{(m)}}{\partial \xi}(x_i, t_j) &= \sum_{p=0}^{N_x}\sum_{q=0}^{N_t} \Phi^{(m)}(x_p, t_q)L_p(x_i)\frac{dL_q(t_j)}{dt} \\
&= \sum_{q=0}^{N_t} \Phi^{(m)}(x_i, t_q)\frac{dL_q(t_j)}{dt} \sum_{q=0}^{N_t}\left(\frac{2}{\xi_m - \xi_{m-1}}\right)\hat{d}_{j,q}\Phi^{(m)}(x_i, t_q) \\
&= \sum_{q=0}^{N_t}\left(\frac{2}{\xi_m - \xi_{m-1}}\right)\hat{d}_{j,q}\Phi_q^{(m)} = \sum_{q=0}^{N_t} d_{j,q}\Phi_q^{(m)},
\end{aligned} \tag{30}$$

where $\hat{d}_{j,q} = \frac{\xi_m - \xi_{m-1}}{2}d_{j,q}$, $j, q = 0, 1, 2, N_t$ are the entries of the standard first order Chebyshev differentiation matrix in the mth subinterval. Substituting Eqs. (28)–(30) into Eqs. (19)–(21), we have:

$$\begin{aligned}
&\left[\mathbf{a}_{0,r}^{(m)}\mathbf{D}^3 + \mathbf{a}_{1,r}^{(m)}\mathbf{D}^2 + \mathbf{a}_{2,r}^{(m)}\mathbf{D} + \mathbf{a}_{3,r}^{(m)}\right]\mathbf{F}_{j,r+1}^{(m)} + \mathbf{a}_{4,r}^{(m)}\sum_{q=0}^{N_t} d_{j,q}\mathbf{D}\mathbf{F}_{q,r+1}^{(m)} \\
&\quad + \mathbf{a}_{5,r}^{(m)}\sum_{q=0}^{N_t} d_{j,q}\mathbf{F}_{q,r+1}^{(m)} = \mathbf{R}_{1,j,r}^{(m)},
\end{aligned} \tag{31}$$

$$\left[\mathbf{b}_{0,r}^{(m)}\mathbf{D}^2+\mathbf{b}_{1,r}^{(m)}\mathbf{D}+\mathbf{b}_{2,r}^{(m)}\right]\mathbf{\Theta}_{j,r+1}^{(m)}+\mathbf{b}_{3,r}^{(m)}\sum_{q=0}^{N_t}d_{j,q}\mathbf{\Theta}_{q,r+1}^{(m)}+\left[\mathbf{b}_{4,r}^{(m)}\mathbf{D}+\mathbf{b}_{5,r}^{(m)}\right]\mathbf{F}_{j,r+1}^{(m)}+\mathbf{b}_{6,r}^{(m)}\sum_{q=0}^{N_t}d_{j,q}\mathbf{F}_{q,r+1}^{(m)}+\left[\mathbf{b}_{7,r}^{(m)}\mathbf{D}\right]\mathbf{\Phi}_{j,r+1}^{(m)}=\mathbf{R}_{2,j,r}^{(m)}, \tag{32}$$

$$\left[\mathbf{c}_{0,r}^{(m)}\mathbf{D}^2+\mathbf{c}_{1,r}^{(m)}\mathbf{D}+\mathbf{c}_{2,r}^{(m)}\right]\mathbf{\Phi}_{j,r+1}^{(m)}+\mathbf{c}_{3,r}^{(m)}\sum_{q=0}^{N_t}d_{j,q}\mathbf{\Phi}_{q,r+1}^{(m)}+\left[\mathbf{c}_{4,r}^{(m)}\mathbf{D}+\mathbf{c}_{5,r}^{(m)}\right]\mathbf{F}_{j,r+1}^{(m)}+\mathbf{c}_{6,r}^{(m)}\sum_{q=0}^{N_t}d_{j,q}\mathbf{F}_{q,r+1}^{(m)}+\left[\mathbf{c}_{7,r}^{(m)}\mathbf{D}^2\right]\mathbf{\Theta}_{j,r+1}^{(m)}=\mathbf{R}_{3,j,r}^{(m)}. \tag{33}$$

Noting that the solution at the time level $j=N_t$ of each sub-interval is given by the solution at the previous level, and taking i and j as dummy indices, Eqs. (31)–(33) can be written as

$$\left[\mathbf{a}_{0,r}^{(m)}\mathbf{D}^3+\mathbf{a}_{1,r}^{(m)}\mathbf{D}^2+\mathbf{a}_{2,r}^{(m)}\mathbf{D}+\mathbf{a}_{3,r}^{(m)}\right]\mathbf{F}_{i,r+1}^{(m)}+\mathbf{a}_{4,r}^{(m)}\sum_{j=0}^{N_t-1}d_{i,j}\mathbf{D}\mathbf{F}_{j,r+1}^{(m)}+\mathbf{a}_{5,r}^{(m)}\sum_{j=0}^{N_t-1}d_{i,j}\mathbf{F}_{j,r+1}^{(m)}=\mathbf{R}_{1,i,r}^{(m)}-\mathbf{a}_{4,r}^{(m)}d_{i,N_t}\mathbf{D}\mathbf{F}_{N_t,r+1}^{(m)}+\mathbf{a}_{5,r}^{(m)}d_{i,N_t}\mathbf{F}_{N_t,r+1}^{(m)}, \tag{34}$$

$$\left[\mathbf{b}_{0,r}^{(m)}\mathbf{D}^2+\mathbf{b}_{1,r}^{(m)}\mathbf{D}+\mathbf{b}_{1,r}^{(m)}\right]\mathbf{\Theta}_{i,r+1}^{(m)}+\mathbf{b}_{3,r}^{(m)}\sum_{j=0}^{N_t-1}d_{i,j}\mathbf{\Theta}_{j,r+1}^{(m)}+\left[\mathbf{b}_{4,r}^{(m)}\mathbf{D}+\mathbf{b}_{5,r}^{(m)}\right]\mathbf{F}_{i,r+1}^{(m)}+\mathbf{b}_{6,r}^{(m)}\sum_{j=0}^{N_t-1}d_{i,j}\mathbf{F}_{j,r+1}^{(m)}+\left[\mathbf{b}_{7,r}^{(m)}\mathbf{D}\right]\mathbf{\Phi}_{i,r+1}^{(m)}=\mathbf{R}_{2,i,r}^{(m)}-\mathbf{b}_{3,r}^{(m)}d_{i,N_t}\mathbf{\Theta}_{N_t,r+1}^{(m)}-\mathbf{b}_{6,r}^{(m)}d_{i,N_t}\mathbf{F}_{N_t,r+1}^{(m)}, \tag{35}$$

$$\left[\mathbf{c}_{0,r}^{(m)}\mathbf{D}^2+\mathbf{c}_{1,r}^{(m)}\mathbf{D}+\mathbf{c}_{2,r}^{(m)}\right]\mathbf{\Phi}_{i,r+1}^{(m)}+\mathbf{c}_{3,r}^{(m)}\sum_{j=0}^{N_t-1}d_{i,j}\mathbf{\Phi}_{j,r+1}^{(m)}+\left[\mathbf{c}_{4,r}^{(m)}\mathbf{D}+\mathbf{c}_{5,r}^{(m)}\right]\mathbf{F}_{i,r+1}^{(m)}+\mathbf{c}_{6,r}^{(m)}\sum_{j=0}^{N_t-1}d_{i,j}\mathbf{F}_{q,r+1}^{(m)}+\left[\mathbf{c}_{7,r}^{(m)}\mathbf{D}^2\right]\mathbf{\Theta}_{i,r+1}^{(m)}=\mathbf{R}_{3,i,r}^{(m)}-\mathbf{c}_{3,r}^{(m)}d_{i,N_t}\mathbf{\Theta}_{N_t,r+1}^{(m)}-\mathbf{c}_{6,r}^{(m)}d_{i,N_t}\mathbf{F}_{N_t,r+1}^{(m)}. \tag{36}$$

In a more compact format, Eqs. (34)–(36) can be written as

$$\mathbf{A}_{1,1}^{(i)}\mathbf{F}_{i,r+1}^{(m)}+\mathbf{a}_{4,r}^{(m)}\sum_{j=0}^{N_t-1}d_{i,j}\mathbf{D}\mathbf{F}_{j,r+1}^{(m)}+\mathbf{a}_{5,r}^{(m)}\sum_{j=0}^{N_t-1}d_{i,j}\mathbf{F}_{j,r+1}^{(m)}+\mathbf{A}_{1,2}^{(i)}\mathbf{\Phi}_{i,r+1}^{(m)}+\mathbf{A}_{1,3}^{(i)}\mathbf{\Theta}_{i,r+1}^{(m)}=\boldsymbol{\beta}_{1,i,r}^{(m)}, \tag{37}$$

$$\mathbf{A}_{2,1}^{(i)}\mathbf{F}_{i,r+1}^{(m)}+\mathbf{b}_{6,r}^{(m)}\sum_{j=0}^{N_t-1}d_{i,j}\mathbf{F}_{j,r+1}^{(m)}+\mathbf{A}_{2,2}^{(i)}\mathbf{\Theta}_{i,r+1}^{(m)}+\mathbf{b}_{3,r}^{(m)}\sum_{j=0}^{N_t-1}d_{i,j}\mathbf{\Theta}_{j,r+1}^{(m)}+\mathbf{A}_{2,3}^{(i)}\mathbf{\Phi}_{i,r+1}^{(m)}=\boldsymbol{\beta}_{2,i,r}^{(m)}, \tag{38}$$

$$\mathbf{A}_{3,1}^{(i)}\mathbf{F}_{i,r+1}^{(m)}+\mathbf{c}_{6,r}^{(m)}\sum_{j=0}^{N_t-1}d_{i,j}\mathbf{F}_{j,r+1}^{(m)}+\mathbf{A}_{3,2}^{(i)}\mathbf{\Theta}_{i,r+1}^{(m)}+\mathbf{A}_{3,3}^{(i)}\mathbf{\Phi}_{i,r+1}^{(m)}+\mathbf{c}_{3,r}^{(m)}\sum_{j=0}^{N_t-1}d_{i,j}\mathbf{\Phi}_{j,r+1}^{(m)}=\boldsymbol{\beta}_{3,i,r}^{(m)}, \tag{39}$$

where

$$\mathbf{A}_{1,1}^{(i)}=\mathbf{a}_{0,r}^{(m)}\mathbf{D}^3+\mathbf{a}_{1,r}^{(m)}\mathbf{D}^2+\mathbf{a}_{2,r}^{(m)}\mathbf{D}+\mathbf{a}_{3,r}^{(m)},\quad \mathbf{A}_{1,2}^{(i)}=0\quad \mathbf{A}_{1,3}^{(i)}=0$$
$$\mathbf{A}_{2,1}^{(i)}=\mathbf{b}_{4,r}^{(m)}\mathbf{D}+\mathbf{b}_{5,r}^{(m)},\quad \mathbf{A}_{2,2}^{(i)}=\mathbf{b}_{0,r}^{(m)}\mathbf{D}^2+\mathbf{b}_{1,r}^{(m)}\mathbf{D},+\mathbf{b}_{2,r}^{(m)}\quad \mathbf{A}_{2,3}^{(i)}=\mathbf{b}_{7,r}^{(m)}\mathbf{D}$$
$$\mathbf{A}_{3,1}^{(i)}=\mathbf{c}_{4,r}^{(m)}\mathbf{D}+\mathbf{c}_{5,r}^{(m)},\quad \mathbf{A}_{3,2}^{(i)}=\mathbf{c}_{7,r}^{(m)}\mathbf{D}^2,\quad \mathbf{A}_{3,3}^{(i)}=\mathbf{c}_{0,r}^{(m)}\mathbf{D}^2+\mathbf{c}_{1,r}^{(m)}\mathbf{D},+\mathbf{c}_{2,r}^{(m)}$$
$$\boldsymbol{\beta}_{1,i,r}^{(m)}=\mathbf{R}_{1,i,r}^{(m)}-\mathbf{a}_{4,r}^{(m)}d_{i,N_t}\mathbf{D}\mathbf{F}_{N_t,r+1}^{(m)}-\mathbf{a}_{5,r}^{(m)}d_{i,N_t}\mathbf{F}_{N_t,r+1}^{(m)},$$
$$\boldsymbol{\beta}_{2,i,r}^{(m)}=\mathbf{R}_{2,i,r}^{(m)}-\mathbf{b}_{3,r}^{(m)}d_{i,N_t}\mathbf{\Theta}_{N_t,r+1}^{(m)}-\mathbf{b}_{6,r}^{(m)}d_{i,N_t}\mathbf{F}_{N_t,r+1}^{(m)},$$
$$\boldsymbol{\beta}_{3,i,r}^{(m)}=\mathbf{R}_{3,i,r}^{(m)}-\mathbf{c}_{3,r}^{(m)}d_{i,N_t}\mathbf{\Phi}_{N_t,r+1}^{(m)}-\mathbf{c}_{6,r}^{(m)}d_{i,N_t}\mathbf{F}_{N_t,r+1}^{(m)}.$$

The boundary conditions given in Eq. (22) when evaluated at the Chebyshev-Gauss-Lobatto collocation points give the following:

$$f_{r+1}^{(m)}(\eta_{N_x},\xi_i)=f_w,\quad \sum_{p=0}^{N_x}\mathbf{D}_{N_x,p}f_{r+1}^{(m)}(N_x,\xi_i)=\lambda,\quad \sum_{p=0}^{N_x}\mathbf{D}_{0,p}f_{r+1}^{(m)}(\eta_p,\xi_i)=1,\quad \theta_{r+1}^{(m)}(\eta_{N_x},\xi_i)=1,\quad \theta_{r+1}^{(m)}(\eta_0,\xi_i)=0,\quad N_b\sum_{p=0}^{N_x}\mathbf{D}_{N_x,p}\phi_{r+1}^{(m)}(N_x,\xi_i)+N_t\sum_{p=0}^{N_x}\mathbf{D}_{N_x,p}\theta_{r+1}^{(m)}(N_x,\xi_i)=0,\quad \phi_{r+1}^{(m)}(\eta_0,\xi_i)=0. \tag{40}$$

4. Results and discussion

The systems of nonlinear partial differential Eqs. (8)–(10), subject to the boundary conditions (11) are solved numerically using a multi-domain (or piecewise or multi-stage) bivariate spectral quasilinearization method. Results are presented for the skin friction coefficient and Nusselt number for different physical parameters that are of interest to the flow model. To ascertain the accuracy of the computed numerical results, comparison is made with the results of Jalil et al. [8], Rosca and Pop [9] and Bachok et al. [48]. The comparison is shown in Table 1 where the results are seen to be in very good agreement. This shows the reliability and accuracy of the numerical approach in this paper.

Fig. 2 shows the effect of the suction parameter $f_w>0$ for both cases $\lambda>1$ and $\lambda<1$. It can be observed that when $\lambda>1$, both the velocity and the momentum boundary layer thicknesses decrease with an increase in the suction parameter while for $\lambda<1$, the velocity profiles increase. An increase in the values of the suction parameter leads to a decrease in the boundary layer thickness. This could be attributed to the fact that when the fluid is removed from the system due to suction, the momentum boundary layer thickness reduces. These findings are consistent with those of Jalil et al. [8] in a related earlier investigation.

Fig. 3 illustrates the effect of the injection parameter $f_w<0$ for both $\lambda>1$ and $\lambda<1$. It can be seen that both the velocity and the momentum boundary-layer thicknesses decrease with an increase in the suction parameter when $\lambda>1$ while for $\lambda<1$, the velocity profiles are enhanced. An increase in the suction parameter leads to a decrease in the boundary-layer thickness. These findings are consistent with those of Jalil et al. [8].

Please cite this article in press as: T.M. Agbaje et al., A numerical study of unsteady non-Newtonian Powell-Eyring nanofluid flow over a shrinking sheet with heat generation and thermal radiation, Alexandria Eng. J. (2016), http://dx.doi.org/10.1016/j.aej.2016.09.006

Table 1 Comparison of the MD-BSQLM approximate solutions of $f''(0,\xi)$, and $-\theta'(0,\xi)$, against those of Refs. [8,9,48] for different values of f_w when $Pr = 1$, $\epsilon = \delta = He = N_R = \xi = 0$ and $\lambda = 0.5$ in the absence of N_t and N_b.

f_w	$f''(\xi,0)$				$-\theta'(\xi,0)$			
	Present	Ref. [8]	Ref. [9]	Ref. [48]	Present	Ref. [8]	Ref. [9]	Ref. [48]
2	0.9251	0.9251	0.9250	0.9251	1.6036	1.6036	1.6035	1.6036
4	1.5030	1.5030	1.5029	1.5030	2.8333	2.8330	2.8330	2.8330
6	2.1233	2.1233	2.1233	2.1233	4.1177	4.1177	4.1177	4.1177
8	2.7627	2.7626	2.7626	2.7627	5.4238	5.4238	5.4238	5.4238
10	3.4116	3.4116	3.4116	3.4116	6.7399	6.7399	6.7399	6.7399
12	4.0659	4.0659	4.0659	4.0659	8.0615	8.0615	8.0614	8.0615
14	4.7236	4.7236	4.7235	4.7236	9.3863	9.3863	9.3862	9.3863
16	5.3833	5.3833	5.3833	5.3833	10.7131	10.7131	10.7130	10.7131
18	6.0446	6.0446	6.0445	6.0446	12.0414	12.0413	12.0413	12.0414
20	6.7069	6.7069	6.7068	6.7069	13.3706	13.3706	13.3706	13.3706
25	8.3656	8.3656	8.3656	8.3656	16.6966	16.6964	16.6965	16.6966
30	10.0270	10.0269	10.0269	10.0270	20.0249	20.0248	20.0249	20.0249
40	13.3536	13.3536	13.3535	13.3536	26.6854	26.6853	26.6853	26.6854
50	16.6829	16.6829	16.6828	16.6829	33.3483	33.3483	33.3483	33.3483

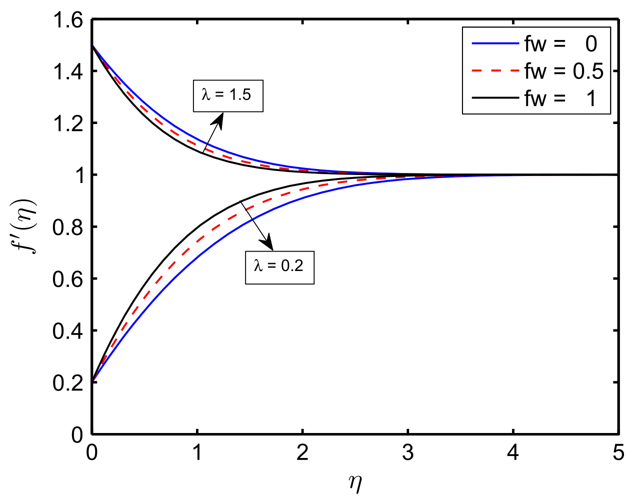

Fig. 2 Velocity profile $f'(\eta)$ for different values of suction parameter $f_w > 0$ when $\delta = 0.1$, $\xi = 1$, $\varepsilon = 0.1$, for both $\lambda = 0.2$ and $\lambda = 1.5$.

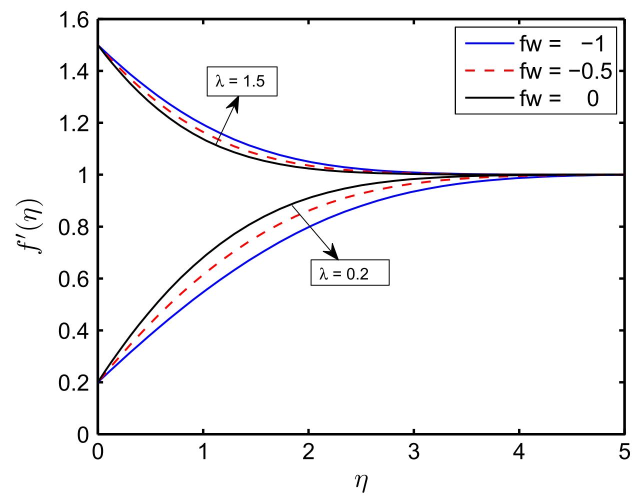

Fig. 3 Velocity profile $f'(\eta)$ for different values of injection parameter $f_w < 0$ when $\delta = 0.1$, $\xi = 1$, $\varepsilon = 0.1$, for both $\lambda = 0.2$ and $\lambda = 1.5$.

The effect of the shrinking parameter λ on the velocity profiles is shown in Fig. 4. We note that for both $\lambda < 0$ and $\lambda > 0$, the velocity profile increases as the shrinking parameter increases. The reason for this could be because an increase in the shrinking parameter increases the nanofluid velocity which in turn increases the momentum boundary layer thickness. These results are in agreement with those obtained by Jalil et al. [8].

Figs. 5 and 6 show the effects of the Powell-Eyring fluid parameters ε, δ, respectively, on the velocity profiles. The velocity profiles decrease and the momentum boundary layer thickness is enhanced as ε and δ increase. This is because Powell-Eyring fluids are shear-thinning fluid such that the viscosity reduces as the shear rate increases. Similar results have been reported in investigations by Jalil et al. [8] and Rocsa and Pop [9].

The influence of suction/injection parameter f_w on the temperature profile is displayed in Fig. 7. It is evident that the tem-

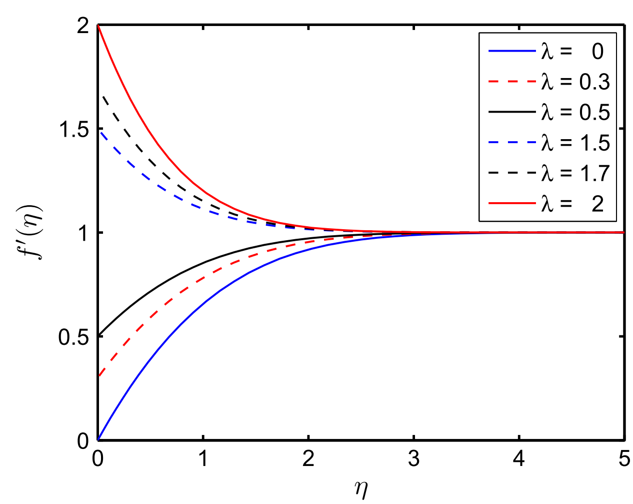

Fig. 4 Velocity profile $f'(\eta)$ for different values of shrinking parameter λ when $\delta = 0.1$, $\xi = 1$, $\varepsilon = 0.1$, and $f_w = 0.5$.

Please cite this article in press as: T.M. Agbaje et al., A numerical study of unsteady non-Newtonian Powell-Eyring nanofluid flow over a shrinking sheet with heat generation and thermal radiation, Alexandria Eng. J. (2016), http://dx.doi.org/10.1016/j.aej.2016.09.006

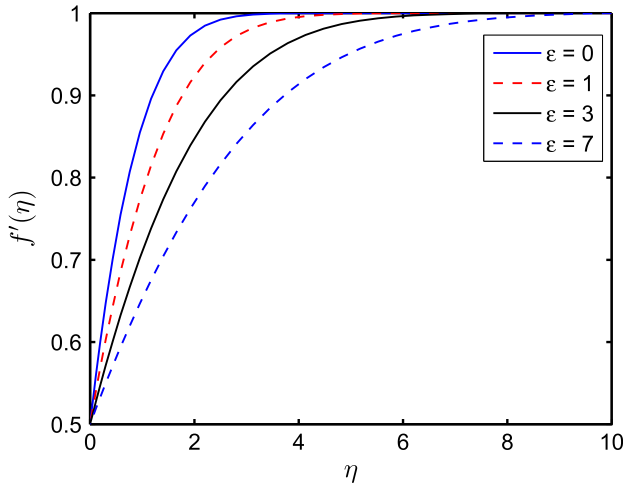

Fig. 5 Velocity profile $f'(\eta)$ for different values of fluid parameter ε when $\delta = 0.1$, $\xi = 1$, $f_w = 0.5$, and $\lambda = 0.5$.

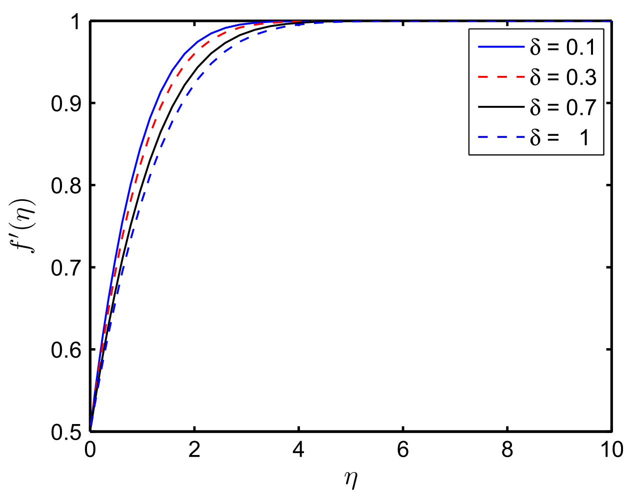

Fig. 6 Velocity profile $f'(\eta)$ for different values of fluid parameter δ when $\varepsilon = 0.1$, $\xi = 1$, $f_w = 0.5$, and $\lambda = 0.5$.

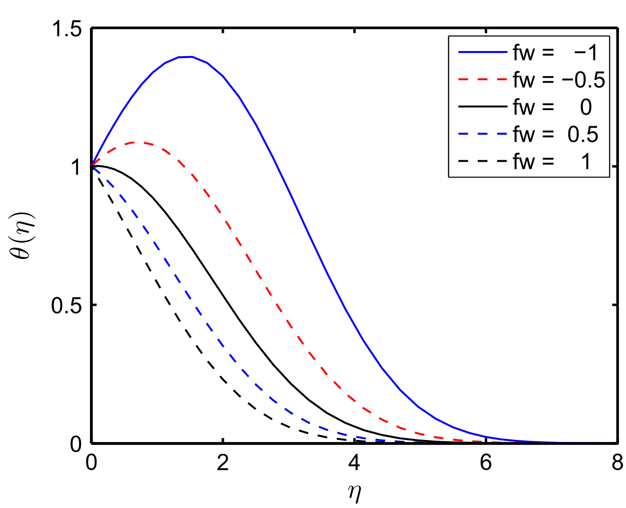

Fig. 7 Temperature profile $\theta(\eta)$ for different values of suction/injection parameter f_w when $\delta = 0.1$, $\xi = \varepsilon = 1$, $He = N_b = N_t = N_R = 0.5$, $Pr = Sc = 1$, and $\lambda = 0.5$.

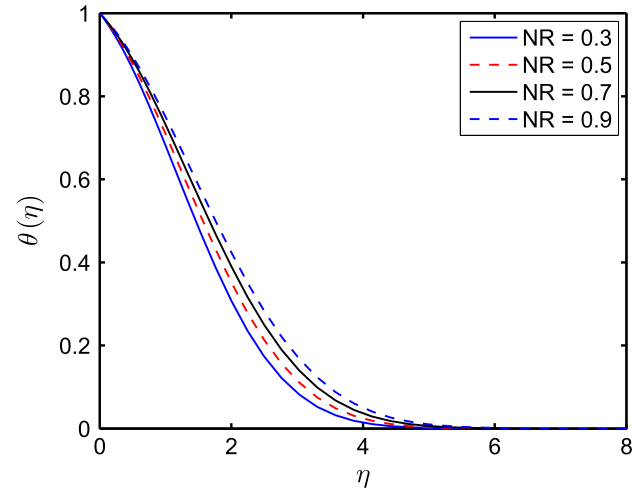

Fig. 8 Temperature profile $\theta(\eta)$ for different values of thermal radiation parameter N_R when $\delta = 0.1$, $\xi = \varepsilon = 1$, $He = N_b = N_t = f_w = 0.5$, $Pr = Sc = 1$, and $\lambda = 0.5$.

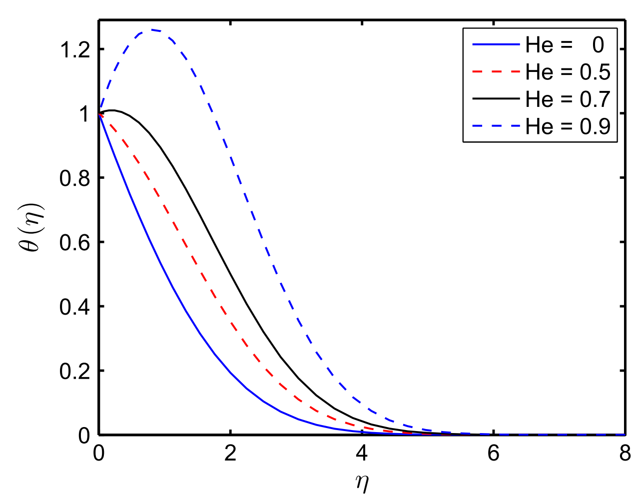

Fig. 9 Temperature profile $\theta(\eta)$ for different values of heat generation parameter He when $\delta = 0.1$, $\xi = \varepsilon = 1$, $f_w = N_b = N_t = N_R = 0.5$, $Pr = Sc = 1$, and $\lambda = 0.5$.

perature and thermal boundary-layer thicknesses reduce with increasing suction/injection parameter values. This is because due to suction, hot fluid is drawn closer to the surface, and as a result, the thermal boundary-layer thickness decreases.

Fig. 8 depicts the influence of the thermal radiation parameter N_R on the temperature profiles. The temperature profiles increase with increasing thermal radiation parameter values. Physically, this may be attributed to the fact that an increase in the thermal radiation parameter yields an increase in the interaction in thermal boundary layer. The effect of heat generation parameter He on temperature profile is displayed in Fig. 9. It is evident that increasing the heat generation parameter increases the temperature profiles, which, in turn leads to an increase in the thermal boundary-layer thickness.

Fig. 10 shows the effect of the thermophoresis parameter N_t on the temperature profiles. It can be seen that the temperature and the thermal boundary-layer thickness increase with an

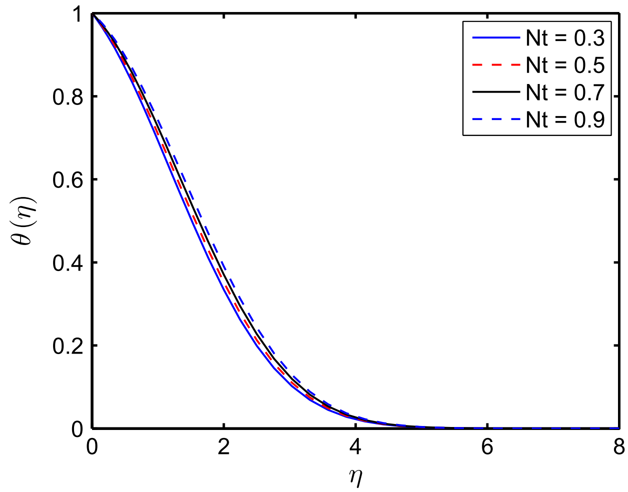

Fig. 10 Temperature profile $\theta(\eta)$ for different values of thermophoresis parameter N_t when $\delta = 0.1$, $\xi = \varepsilon = 1$, $f_w = N_b = He = N_R = 0.5$, $Pr = Sc = 1$, and $\lambda = 0.5$.

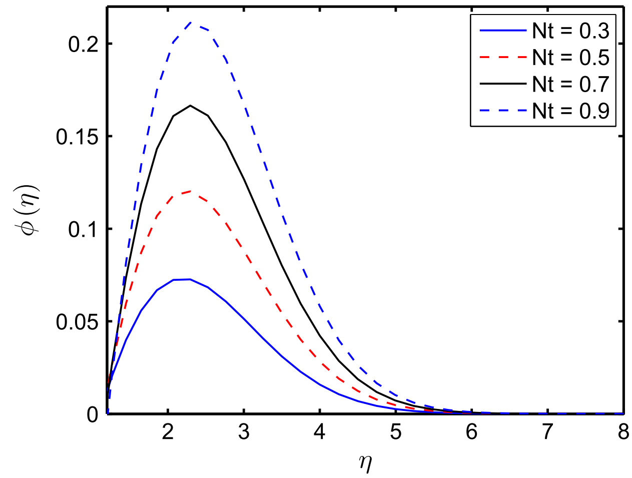

Fig. 12 Concentration profile $\phi(\eta)$ for different values of thermophoresis parameter N_t when $\delta = 0.1$, $\xi = \varepsilon = 1$, $f_w = N_b = He = N_R = 0.5$, $Pr = Sc = 1$, and $\lambda = 0.5$.

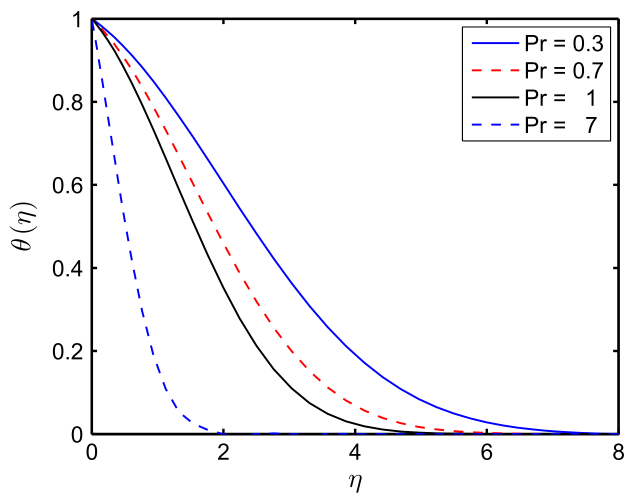

Fig. 11 Temperature profile $\theta(\eta)$ for different values of Prandtl number Pr when $\delta = 0.1$, $\xi = \varepsilon = 1$, $f_w = N_b = N_t = He = N_R = 0.5$, $Sc = 1$, and $\lambda = 0.5$.

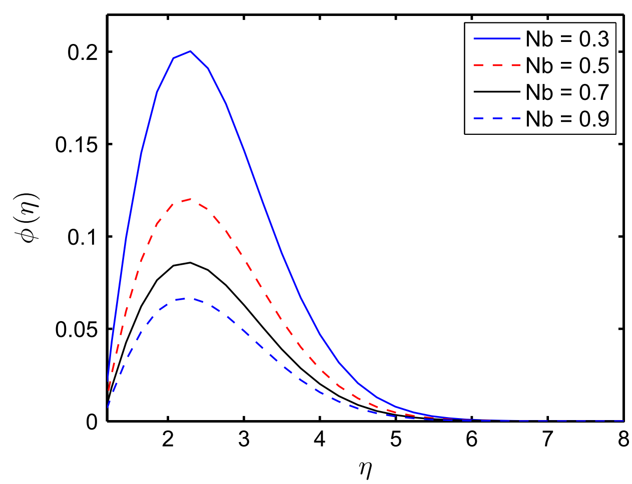

Fig. 13 Concentration profile $\phi(\eta)$ for different values of Brownian motion parameter N_b when $\delta = 0.1$, $\xi = \varepsilon = 1$, $f_w = N_t = He = N_R = 0.5$, $Pr = Sc = 1$, and $\lambda = 0.5$.

increase in the thermophoresis parameter. In Fig. 11 we demonstrate the effect of changes in the Prandtl number Pr on the temperature profiles. The temperature and thermal boundary layer thickness decrease with increasing Prandtl numbers. The effect is more obvious with smaller Prandtl numbers because as the boundary layer becomes thicker, the heat transfer rate reduces. It is generally understood in the literature that fluids with low Prandtl numbers such as liquid metals have a high conductivity, resulting in large thermal boundary-layers. In this case heat diffuses rapidly from the heated plate compared to the case of fluids with high Prandtl numbers.

Figs. 12 and 13 show how the concentration profiles vary with the thermophoresis parameter N_t and the Brownian motion parameter N_b. Fig. 12 shows an increase in the concentration and solutal boundary layer thickness with increase in thermophoresis parameter, while a decrease in the concentration and solutal boundary layer thickness is observed in Fig. 13 with increasing values of Brownian motion parameter.

5. Conclusion

We have investigated the flow of an unsteady Powell-Eyring nanofluid flow over a shrinking sheet with heat generation and thermal radiation effects. Approximate numerical results of the partial differential equations were obtained using a multi-domain (or piecewise or multi-stage) bivariate spectral quasilinearization method. The results from this study show that the fluid parameters ε and δ reduce the flow velocity and the momentum boundary-layer thickness. The heat generation and thermal radiation parameter are found to enhance both the temperature and thermal boundary-layer thickness. These observations are consistent with earlier findings in the literature. The method used proved to be reliable and easy to use, thereby making it a good numerical tool for solving nonlinear PDEs that arise in the boundary-layer studies.

Acknowledgment

The authors are grateful to the University of KwaZulu-Natal, the DST-NRF Centre of Excellence in Mathematical and Statistical Sciences (CoE-MaSS) and the Claude Leon Foundation, South Africa, for necessary financial support.

References

[1] J. Harris, Rheology and Non-Newtonian Flow, Longman, 1977.
[2] R.B. Bird, C.F. Curtis, R.C. Armstrong, O. Hassager, Dynamics of Polymetric Liquids, Wiley, 1987.
[3] R.E. Powell, H. Erying, Nature, London, 1944.
[4] M.Y. Malik, I. Khan, A. Hussain, T. Salahuddin, Mixed convection flow of MHD Eyring-Powell nanofluid over a stretching sheet: a numerical study, AIP Adv. 5 (2015) 117118.
[5] T. Hayat, S. Asad, M. Mustafa, A. Alsaedi, Radiation effects on the flow of Powell-Eyring fluid past an unsteady inclined stretching sheet with non-uniform heat source/sink, Plos One 9 (2014) e103214.
[6] H. Zaman, M.A. Shah, M. Ibrahim, Unsteady incompressible Couette flow problem for the Eyring-Powell model with porous walls, Am. J. Comput. Math. 3 (2013) 313.
[7] S. Nadeem, S. Saleem, Series solution of unsteady Eyring Powell nanofluid flow on a rotating cone, Am. J. Comput. Math. 52 (2015) 725–737.
[8] M. Jalil, S. Asghar, S.M. Imran, Self similar solutions for the flow and heat transfer of Powell-Eyring fluid over a moving surface in a parallel free stream, Int. J. Heat Mass Transfer 65 (2013) 73–79.
[9] A.V. Roşca, I. Pop, Flow and heat transfer of Powell-Eyring fluid over a shrinking surface in a parallel free stream, Int. J. Heat Mass Transfer 71 (2014) 321–327.
[10] T. Hayat, Z. Iqbal, M. Qasim, S. Obaidat, Steady flow of an Eyring Powell fluid over a moving surface with convective boundary conditions, Int. J. Heat Mass Transfer 55 (2012) 1817–1822.
[11] T. Hayat, S. Ali, M.A. Farooq, A. Alsaedi, On comparison of series and numerical solutions for flow of Eyring-Powell fluid with newtonian heating and internal heat generation/absorption, PloS One 10 (2015) e0129613.
[12] A. Asmat, N.A. Khan, H. Khan, F. Sultan, Radiation effect on boundary layer flow of an Eyring-Powell fluid over an exponentially shrinking sheet, Ain Shams Eng. J. 5 (2014) 1337–1342.
[13] N.A. Khan, F. Sultan, On the double diffusive convection flow of Eyring-Powell fluid due to cone through a porous medium with Soret and Dufour effects, AIP Adv. 5 (2015) 057140.
[14] S. Nadeem, S. Saleem, Mixed convection flow of Eyring-Powell fluid along a rotating cone, Results Phys. 4 (2014) 54–62.
[15] S.U.S. Chol, Enhancing thermal conductivity of fluids with nanoparticles, ASME-Publ.-Fed. 231 (1995) 99–106.
[16] J. Buongiorno, Convective transport in nanofluids, J. Heat Transfer 128 (2006) 240–250.
[17] A.M. Rohni, S. Ahmad, A.I.M. Ismail, I. Pop, Flow and heat transfer over an unsteady shrinking sheet with suction in a nanofluid using Buongiorno's model, Int. Commun. Heat Mass Transfer 43 (2013) 75–80.
[18] K. Zaimi, A. Ishak, I. Pop, Unsteady flow due to a contracting cylinder in a nanofluid using Buongiornos model, Int. J. Heat Mass Transfer 68 (2014) 509–513.
[19] R. Dhanai, P. Rana, L. Kumar, Multiple solutions of MHD boundary layer flow and heat transfer behavior of nanofluids induced by a power-law stretching/shrinking permeable sheet with viscous dissipation, Powder Technol. 273 (2015) 62–70.
[20] N.A. Haroun, P. Sibanda, S. Mondal, S.S. Motsa, On unsteady MHD mixed convection in a nanofluid due to a stretching/shrinking surface with suction/injection using the spectral relaxation method, Bound. Val. Probl. 1 (2015) 1–17, http://dx.doi.org/10.1186/s13661-015-0289-5.
[21] N.A.H. Haroun, P. Sibanda, S. Mondal, S.S. Motsa, M.M. Rashidi, Heat and mass transfer of nanofluid through an impulsively vertical stretching surface using the spectral relaxation method, Bound. Val. Probl. 161 (2015) 1–16, http://dx.doi.org/10.1186/s13661-015-0424-3.
[22] N.A.H. Haroun, S. Mondal, P. Sibanda, Unsteady natural convective boundary-layer flow of MHD nanofluid over a stretching surfaces with chemical reaction using the spectral relaxation method: a revised model, Proc. Eng. 127 (2015) 18–24.
[23] N. Dalir, M. Dehsara, S.S. Salman, Entropy analysis for magnetohydrodynamic flow and heat transfer of a Jeffrey nanofluid over a stretching sheet, Energy 79 (2015) 351–362.
[24] M.H. Abolbashari, N. Freidoonimehr, F. Nazari, M.M. Rashidi, Analytical modeling of entropy generation for Casson nano-fluid flow induced by a stretching surface, Adv. Powder Technol. 26 (2015) 542–552.
[25] H. Heidary, R. Pirmohammadi, M.J. Kermani, Numerical study of magnetic field effect on nano-fluid forced convection in a channel, J. Magn. Magn. Mater. 374 (2015) 11–17.
[26] S. Mansur, A. Ishak, I. Pop, The magnetohydrodynamic stagnation point flow of a nanofluid over a stretching/shrinking sheet with suction, PLoS One 10 (2015) e0117733.
[27] R.U. Haq, S. Nadeem, N.S. Akbar, Z.H. Khan, Radiation effect on stagnation point flow of micropolar nanofluid along a vertically convective stretching surface, IEEE Trans. Nanotechnol. 14 (2015) 42–50.
[28] R. Mehmood, S. Nadeem, N. Sher Akbar, Non aligned Ethylene-Glycol 30 percent based stagnation point fluid over a stretching surface with hematite Nano particles, J. Appl. Fluid Mech. 9 (3) (2016) 1359–1366.
[29] N. Sher Akbar, A. Ebaid, Z.H. Khan, Numerical analysis of magnetic field on Eyring-Powell fluid flow towards a stretching sheet, J. Magn. Magn. Mater. 382 (2015) 355–358.
[30] N. Sher Akbar, Z.H. Khan, Effect of variable thermal conductivity and thermal radiation on the flow of CNTS over a stretching sheet with convective slip boundary conditions: Numerical study, J. Mol. Liq. 222 (2016) 279–286.
[31] N. Sher Akbar, Z.H. Khan, Magnetic field analysis in a suspension of gyrotactic microorganisms and nanoparticles over a stretching surface, J. Magn. Magn. Mater. 378 (2016) 320–326.
[32] N. Sher Akbar, Z. Khan, S. Nadeem, W. khan, Double-diffusive natural convective boundary-layer flow of a nanofluid over a stretching sheet with magnetic field, Int. J. Numer. Meth. Heat Fluid Flow 26 (1) (2016) 108–121.
[33] H.S. Nik, S. Effati, S.S. Motsa, S. Shateyi, A new piecewise-spectral homotopy analysis method for solving chaotic systems of initial value problems, Math. Probl. Eng. 2013 (2013) 13, http://dx.doi.org/10.1155/2013/583193. Article ID 583193.
[34] S. Effati, H. Saberi Nik, A. Jajarmi, Hyperchaos control of the hyperchaotic Chen system by optimal control design, Nonlinear Dyn. 73 (2013) 499–508.
[35] J.I. Ramos, Piecewise homotopy methods for nonlinear ordinary differential equations, Appl. Math. Comput. 198 (2008) 92–116.
[36] Z.M. Odibat, C. Bertelle, M.A. Aziz-Alaoui, G.H.E. Duchamp, A multi-step differential transform method and application to non-chaotic or chaotic systems, Comput. Math. Appl. 59 (2010) 1462–1472.

[37] A. Freihat, S. Momani, Adaptation of differential transform method for the numeric-analytic solution of fractional-order Rssler chaotic and hyperchaotic systems, Abstr. Appl. Anal. 2012 (2012) 13, http://dx.doi.org/10.1155/2012/934219. Article ID 934219.

[38] O. Abdulaziz, N.F.M. Noor, I. Hashim, M.S.M. Noorani, Further accuracy tests on Adomian decomposition method for chaotic systems, Chaos Soliton. Fract. 36 (2008) 1405–1411.

[39] M.M. Al-Sawalha, M.S.M. Noorani, I. Hashim, On accuracy of Adomian decomposition method for hyperchaotic Rossler system, Chaos Soliton. Fract. 40 (2009) 1801–1807.

[40] S.S. Motsa, A new piecewise-quasilinearization method for solving chaotic systems of initial value problems, Open Phys. 10 (2012) 936–946.

[41] S.S. Motsa, P. Sibanda, A multistage linearisation approach to a four-dimensional hyperchaotic system with cubic nonlinearity, Nonlinear Dyn. 70 (2012) 651–657.

[42] S.S. Motsa, P. Dlamini, M. Khumalo, A new multistage spectral relaxation method for solving chaotic initial value systems, Nonlinear Dyn. 72 (2013) 265–283.

[43] H.S. Nik, P. Rebelo, Multistage spectral relaxation method for solving the hyperchaotic complex systems, Sci. World J. 2014 (2014) 10, http://dx.doi.org/10.1155/2012/934219. Article ID 943293.

[44] S.S. Motsa, On the bivariate spectral homotopy analysis method approach for solving nonlinear evolution partial differential equations, Abstr. Appl. Anal. 2014 (2014) 8, http://dx.doi.org/10.1155/2014/350529. Article ID 350529.

[45] S.S. Motsa, V.M. Magagula, P. Sibanda, A bivariate Chebyshev spectral collocation quasilinearization method for nonlinear evolution parabolic equations, Sci. World J. 2014 (2014) 13, http://dx.doi.org/10.1155/2014/581987. Article ID 581987.

[46] V.M. Magagula, S.S. Motsa, P. Sibanda, P.G. Dlamini, On a bivariate spectral relaxation method for unsteady magneto-hydrodynamic flow in porous media, SpringerPlus 5 (2016) 1–15, http://dx.doi.org/10.1186/s40064-016-2053-4.

[47] R.E. Bellman, R.E. Kalaba, Quasilinearization and Nonlinear Boundary-Value Probl, Elsevier Publishing Company, New York, 1965.

[48] N. Bachok, M.A. Jaradat, I. Pop, A similarity solution for the flow and heat transfer over a moving permeable flat plate in a parallel free stream, Heat Mass Transfer 47 (2001) 1643–1649.

[49] I.S. Oyelakin, S. Mondal, P. Sibanda, Unsteady Casson nanofluid flow over a stretching sheet with thermal radiation, convective and slip boundary conditions, Alex. Eng. J. 55 (2016) 1025–1035.

[50] L.N. Trefethen, Spectral Methods in MATLAB, SIAM, Philadelphia, 2000.

[51] C. Canuto, M.Y. Hussaini, A. Quarteroni, T.A. Zang, Spectral Methods in Fluid Dynamics, Springer-Verlag, Berlin, 1988.

Please cite this article in press as: T.M. Agbaje et al., A numerical study of unsteady non-Newtonian Powell-Eyring nanofluid flow over a shrinking sheet with heat generation and thermal radiation, Alexandria Eng. J. (2016), http://dx.doi.org/10.1016/j.aej.2016.09.006